










Cite this: *Nanoscale*, 2019, **11**, 541

[^{99m}Tc-HYNIC-*N*-dodecylamide]: a new hydrophobic tracer for labelling reconstituted high-density lipoproteins (rHDL) for radioimaging†

Keila Isaac-Olivé, *^a Blanca E. Ocampo-García, ^b Liliana Aranda-Lara, ^a Clara L. Santos-Cuevas, ^b Nallely P. Jiménez-Mancilla, ^b Myrna A. Luna-Gutiérrez, ^b Luis. A. Medina, ^c Bhavani Nagarajan,^d Nirupama Sabnis,^d Sangram Raut, *^d Laszlo Prokai *^e and Andras G. Lacko*^d

Despite the widespread use of nanotechnology in radio-imaging applications, lipoprotein based delivery systems have received only limited attention so far. These studies involve the synthesis of a novel hydrophobic radio-imaging tracer consisting of a hydrazinonicotinic acid (HYNIC)-*N*-dodecylamide and ^{99m}Tc conjugate that can be encapsulated into rHDL nanoparticles (NPs). These rHDL NPs can selectively target the Scavenger Receptor type B1 (SR-B1) that is overexpressed on most cancer cells due to excess demand for cholesterol for membrane biogenesis and thus can target tumors *in vivo*. We provide details of the tracer synthesis, characterization of the rHDL/tracer complex, *in vitro* uptake, stability studies and *in vivo* application of this new radio-imaging approach.

Received 13th September 2018,

Accepted 16th November 2018

DOI: 10.1039/c8nr07484d

rsc.li/nanoscale

Introduction

Radio-imaging agents, including ^{99m}Tc, play an important role in oncology, in the early diagnosis of tumors. The development of delivery systems for the selective and efficient transport of these radio-imaging agents to the tumor site is a key area of current radiopharmaceutical research. Several NPs have been evaluated to enhance the pharmacokinetics and bio-distribution of imaging agents.^{1–4} Nevertheless, more work is needed to improve tumor targeting and contrast, especially for prostate and breast cancer imaging.^{5,6} The specific NPs with the capacity to accommodate hydrophobic substances, upon assembly, such as liposomes,⁷ have been used extensively in molecular imaging studies. Another NP platform with a hydrophobic core, rHDL

NPs, also appears suitable for this task as it has already been employed in the imaging of atherosclerotic plaques.^{8,9}

Endogenous plasma HDL are complex structures of 5 to 12 nm in diameter, containing an apolar core of primarily esterified cholesterol that is coated by phospholipids, free cholesterol, and protein components, including apolipoprotein A-1 (Apo A-1). The complex of non-polar and polar lipids is held together by the Tre-foil structure of apolipoproteins, as modeled by lipid complexes with Apo A-I.^{10,11} This molecular complex is responsible for initiating reverse cholesterol transport from peripheral tissues, facilitating the transport of esterified cholesterol to the liver for excretion. The delivery mechanism involves the recognition of Apo A-1 by the extracellular domain of the scavenger receptor type B1 (SR-B1), present in the hepatocyte plasma membrane.^{12,13} Unlike many other nanoparticle platforms, the Apo A-1/SR-B1 interaction leads to the intracellular (cytoplasmic) delivery of esterified cholesterol without endocytosis of the whole HDL particle.¹⁴ As a result, HDL with a reduced cholesterol content returns to the bloodstream (*via* retro-endocytosis) to acquire more cholesterol.¹⁵

Synthetic or reconstituted HDL (rHDL) NPs have been utilized to deliver anti-cancer agents to cancer cells and to malignant tumors as they are structurally and functionally similar to endogenous HDL.¹⁶ Studies by us and several other investigators have reported SR-B1 receptor overexpression in cancer cells and tumors.^{12,13,17–19} This overexpression is consistent with the sustained and increasing demand for cholesterol (it is essential for building the cell membrane) upon extracting it

^aFacultad de Medicina, Universidad Autónoma del Estado de México, Toluca, 50180 Estado de México, Mexico. E-mail: kisaaco@uaemex.mx

^bInstituto Nacional de Investigaciones Nucleares, Ocoyoacac 52750, Estado de México, Mexico

^cInstituto de Física, Universidad Nacional Autónoma de México, Ciudad de México, Mexico/Unidad de Investigación Biomédica en Cáncer INCAN-UNAM, Instituto Nacional de Cancerología, Ciudad de México, Mexico

^dDept. of Physiology and Anatomy, University of North Texas Health Science Center, Fort Worth, TX 76107, USA. E-mail: sangram.raut@unthsc.edu, andras.lacko@unthsc.edu

^eDept. of Pharmacology and Neuroscience, University of North Texas Health Science Center, Fort Worth, TX 76107, USA. E-mail: laszlo.prokai@unthsc.edu

†Electronic supplementary information (ESI) available. See DOI: 10.1039/c8nr07484d

from plasma HDL.²⁰ The acquisition of excess cholesterol by malignant tissues leads to reduced plasma HDL-Cholesterol (HDL-C) levels in cancer patients as observed by several studies.^{21–25} Consequently, HDL type NPs appear suitable for therapeutic delivery vehicles for drugs and imaging agents.²⁶

This interaction between rHDL and the SR-B1 receptor has been used for the transportation and specific release of drugs and imaging agents to cancer cells. Therapeutic agents such as paclitaxel, valrubicin (chemotherapy¹⁸), siRNA (gene therapy),²⁷ gold NPs (photothermal therapy and contrast agent in CT imaging),²⁸ free radical-producing fluorophores such as curcumin (photodynamic therapy),^{29,30} gadolinium, magnetic NPs (NMR contrast agent imaging),⁹ and quantum dots (optical imaging)³¹ have been incorporated into the lipid core of HDL (similar to esterified cholesterol), to function as a “Trojan Horse”^{12,13} transporting the encapsulated agent selectively to the cytoplasm of cancer cells and tumors. Most of the earlier studies involved the delivery of imaging agents to atherosclerotic lesions, employing animal models,^{8,9,32} and consequently more work with tumor models is needed to facilitate the enhancement of tumor imaging using rHDL NPs.

Despite the widespread clinical use of nuclear imaging techniques, so far, there have been very few reports on HDL (or HDL type NPs) as delivery vehicles for tumor imaging agents. One example of such a study involved HDL radiolabeled with the radionuclide ⁸⁹Zr for PET imaging of breast tumors.³³ Other reports described the labeling of low density lipoproteins (LDL) where the surface of the nanoparticle was altered for the imaging approach.^{34,35} As mentioned earlier, HDL type NPs have been mainly studied as drug delivery agents, primarily against malignant tumors. Although their medical imaging and theranostic potential have been discussed,³⁶ given the high sensitivity of nuclear imaging, it would be desirable to have a ^{99m}Tc based tracer complex available for the evaluation of rHDL nanocarriers *in vivo*. However, currently, no studies have been reported on rHDL radiolabeled with ^{99m}Tc (radionuclide SPECT) even though it is the most widely used radionuclide in imaging studies for nuclear medicine (approximately 30 million studies performed per year with ^{99m}Tc).

One of the possible strategies for the preparation of ^{99m}Tc-rHDL was to bind the radionuclide through a bifunctional linker to the surface of the rHDL (link to apo-A1, or to phospholipids), and in this way the images obtained were expected to take advantage of the overexpression of SR-B1 receptors. However, to take advantage of the interaction of Apo A-1 with SR-B1, another labeling strategy was utilized here to internalize the isotopic label in the phospholipid layer (or perhaps in the interior core) of the rHDL NPs. Thus, the hydrophobic tracer would be selectively released and accumulated in the cytoplasm of the cancer cell, without going through endocytosis.³¹

The objective of these studies was to synthesize a hydrophobic derivative of hydrazino-nicotinic acid (HYNIC) in order to prepare a conjugate, based on the HYNIC/EDDA/tricine structure that can be encapsulated with high efficiency into the lipid core of HDL and be transported and internalized by prostate cancer (PC3) cells with the aim of visualizing the tumor.

Satisfactory evaluation of this radio-pharmaceutical would then be pursued for potential clinical application, to reveal the contour of the prostate tumors with enhanced contrast. These studies are important in light of growing interest in the area of theranostics; combined imaging and therapy.^{37–39}

Materials and methods

Chemicals, supplies, and instruments

Chemicals (egg yolk phosphatidylcholine, free cholesterol and cholesterol ester) needed for rHDL synthesis were ordered from Sigma Aldrich. Apolipoprotein A1 was ordered from MC Labs, South San Francisco, CA. Dodecylamine and anhydrous 1-hydroxybenzotriazole were obtained from ACROS Organics (Geel, Belgium) and AnaSpec (Fremont, CA), respectively. All other chemicals were obtained from Sigma-Aldrich (St Louis, MO, USA). Reactions were performed using a Wheaton (Millville, NJ, USA) micro kit, and isolation of the reaction products was performed using commercial labware. Melting points (m.p.) were determined using an electrothermal apparatus (Mel-Temp®, Barnstead International, Dubuque, IA, USA) and reported without correction. Mass spectra were recorded on a linear ion trap (LTQ) and a linear ion trap–Orbitrap (LTQ Velos Orbitrap Pro) hybrid instrument (both from Thermo Fisher Scientific, San Jose, CA, USA) using an atmospheric pressure solids analysis probe (ASAP; M&M Mass Spec Consulting, Newark, DE, USA) as described in the literature.⁴⁰ For accurate-mass measurements by using the Orbitrap, nominal resolution ($M/\Delta M$, at m/z 400) was set to 50 000 and internal calibration was done after acquisition using RecalOffline (version 2.2.0115) and protonated dioctyl phthalate (m/z 391.2843) as a reference ion.⁴¹ ¹H nuclear magnetic resonance (NMR) spectra were obtained at 300 MHz on a Bruker (Billerica, MA, USA) Fourier 300 HD instrument in dimethyl-*d*₆ sulfoxide (DMSO-*d*₆) containing tetramethylsilane as an internal reference.

Synthesis of HYNIC-*N*-dodecylamide

The synthesis was carried out in two steps, starting from 6-chloropyridine-3-carboxylic acid. The first step was the reaction with dodecylamine to form the amide as shown in Fig. 1.

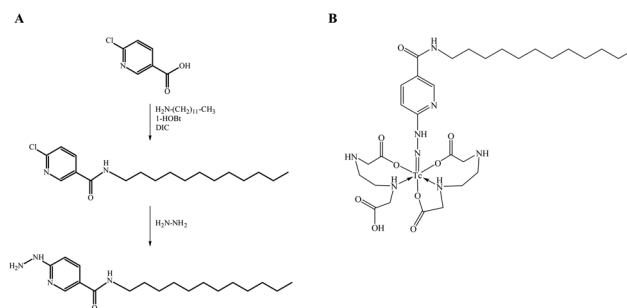


Fig. 1 (A) Scheme for the synthesis of 6-hydrazinopyridine-3-carboxylic acid dodecylamide (HYNIC-DA). (B) Coordination chemistry of ^{99m}Tc with HYNIC-DA and EDDA.⁴⁶

The second reaction involved the substitution of 6-Cl by hydrazine to form 6-hydrazinopyridine-3-carboxylic acid dodecylamide (HYNIC-DA). Fig. 1B also shows the coordination chemistry for ^{99m}Tc -radioisotope.

6-Chloropyridine-3-carboxylic acid dodecylamide

Dodecylamine (0.93 g, 5 mmol), 6-chloropyridine-3-carboxylic acid (0.79 g, 5 mmol) and anhydrous 1-hydroxybenzotriazole (1-HOBT; 0.75 g, 5.6 mmol) were dissolved in 3 mL dichloromethane. After the addition of *N,N'*-diisopropylcarbodiimide (DIC; 860 μl \sim 0.70 g, 5.6 mmol), the reaction vial was capped and the mixture was stirred overnight at room temperature using a Teflon[®]-coated cylindrical magnetic bar and a laboratory stirrer/hot plate (Corning, Acton, MA, USA). Completion of the reaction was confirmed by ASAP mass spectrometry. The crude product was isolated by vacuum filtration, and was recrystallized from dichloromethane. Off-white solid, 1.25 g (\sim 75% yield); m.p. 100 $^{\circ}\text{C}$; ASAP-MS: m/z 325 and 327 (for ^{35}Cl and ^{37}Cl isotopes, respectively, \sim 3 : 1 ratio of ion abundance); HR-MS: m/z 325.2037, $\Delta = -1.3$ ppm for $\text{C}_{18}\text{H}_{30}\text{N}_2\text{O}^{35}\text{Cl}$ (MH^+) and 327.2010, $\Delta = -0.5$ ppm for $\text{C}_{18}\text{H}_{30}\text{N}_2\text{O}^{37}\text{Cl}$ (MH^+); $^1\text{H-NMR}$ (δ , ppm): 8.81 (s, $J = 0.6$ Hz, 1H, pyridinium H-2), 8.22 (d, $J = 8.4$ and 0.9 Hz, 1H, pyridinium H-4), 7.64 (d, $J = 8.4$ Hz, 1H, pyridinium H-5), 3.26 (dt, $J = 7.8$ and 6.8 Hz, 2H, α -CH₂ of dodecylamide), 1.51 (m, 2H, β -CH₂ of dodecylamide), 1.20–1.32 (bs, 18H, γ -CH₂ to λ -CH₂ of dodecylamide), 0.87 (t, $J = 6.2$ Hz, 3H, CH₃ of dodecylamide).

6-Hydrazinopyridine-3-carboxylic acid dodecylamide (hydrazinonicotinoic acid dodecylamide, HYNIC-DA)

To the isolated 6-chloropyridine-3-carboxylic acid dodecylamide (1 g, \sim 3 mmol), two mL of reagent alcohol was added into a 10 mL reaction vial fitted with a water-cooled jacketed condenser. The mixture was brought to reflux under stirring using the stirrer/hot plate (from Corning, see the previous paragraph) and a Teflon[®]-coated cylindrical magnetic bar. Then, 0.5 mL of hydrazine/water solution (85/15, v/v) was added drop-wise through the condenser using a disposable glass pipette, and the reaction was allowed to proceed under reflux for 2 hours. Completion of the reaction was confirmed by ASAP mass spectrometry. After cooling, the suspension was poured into 5 mL of ice-cold water, and the product was isolated by vacuum filtration followed by washing with water and, then, 1% HCl solution (w/v) 5 mL each, followed by drying the isolated product in a vacuum desiccator. Grey-white solid, 0.52 g (\sim 50% yield); m.p. 208 $^{\circ}\text{C}$; ASAP-MS: m/z 321; HR-MS: m/z 321.2639, $\Delta = -3.0$ ppm for $\text{C}_{18}\text{H}_{33}\text{N}_4\text{O}$ (MH^+); $^1\text{H-NMR}$ (δ , ppm): 8.60 (d, $J = 2.0$ Hz, 1H, pyridinium H-2), 8.12 (dd, $J = 8.8$ and 2.0 Hz, 1H, pyridinium H-4), 6.91 (d, $J = 8.8$ Hz, 1H, pyridinium H-5), 3.23 (dt, $J = 8.0$ and 6.8 Hz, 2H, α -CH₂ of dodecylamide), 1.50 (p, $J = 8.0$ Hz, 2H, β -CH₂ of dodecylamide), 1.24–1.28 (bs, 18H, γ -CH₂ to λ -CH₂ of dodecylamide), 0.85 (t, $J = 7.0$ Hz, 3H, CH₃ of dodecylamide).

Liposome and rHDL preparation and characterization

Liposome preparation. Chemicals were purchased from Avanti Polar Lipids, Inc. (Alabaster, AL, USA). Liposomes were

prepared according to the method reported by Toro-Córdova *et al.*⁴² which is a variation of the reverse-phase evaporation method reported in the literature.⁴³ Briefly, the lipid combination soybean 1- α -phosphatidylcholine (HSPC); 1,2-distearoyl-*sn*-glycero-3-phosphoethanolamine-*N*-[methoxy(polyethylene glycol)-2000] (DSPE-mPEG2000); and cholesterol in a ratio of HSPC : DSPE-mPEG2000 : cholesterol (60% : 5% : 35%) was dissolved in chloroform : methanol (2 : 1) and added dropwise to double distilled water (DDW) at 70 $^{\circ}\text{C}$. The resulting mixture was subjected to fast agitation to produce a water-in-oil emulsion. Solvents were evaporated in a round flask under sonication resulting in the formation of liposomes. The particle size was reduced by sonication and homogenization by passing once through various membrane filters (once through 400 nm membrane, twice through a 200 nm membrane and four times through a 100 nm membrane). Liposomes were finally suspended in a known DDW volume.

Liposome characterization. The physicochemical characterization of liposomes included the phospholipid quantification, determination of particle size and zeta potential. Phospholipid determination in the final liposome suspension was done by the Stewart method.⁴⁴ Particle size and zeta potential measurements (5 repetitions) of the colloidal solution were carried out using a particle size (dynamic light scattering) and Z potential analyzer (Nanotrac Wave, Model MN401, Microtract, FL, USA).

rHDL preparation. rHDL synthesis was accomplished by a procedure developed earlier.¹⁸ Briefly, a mixture of egg yolk phosphatidylcholine (EYPC), free cholesterol (FC), and cholesterol oleate (CE) was prepared in chloroform. The lipid mixture (EYPC, FC, and CE) was dried under nitrogen to a thin film and dispersed in 60 μL DMSO. To this mixture, Apo A-I (5 mg) and 140 μL sodium cholate (from a stock of 100 mM) were added and the volume was made up to 2 mL with tris-ethylenediaminetetraacetic acid (EDTA) buffer (10 mM Tris, 0.1 M KCl, 1 mM EDTA pH 8.0). The final EYPC to cholate molar ratio was maintained at (1 : 1.6). The lipid/protein/cholate mixture was then incubated for 12 h at 4 $^{\circ}\text{C}$, followed by dialysis against 2 L of phosphate buffer saline (PBS) for 48 h with three buffer changes in the first 12 h. The preparations were then centrifuged at 1000 rpm for 2 min and filtered using a 0.2 μm syringe filter. The preparations were kept in the dark at 4 $^{\circ}\text{C}$ until further use.

rHDL characterization. The phospholipid content was determined by using an enzymatic reagent kit (phospholipid C) using microtiter plate assays as per the manufacturer's suggestions. Protein determinations were carried out using a BCA protein assay kit. Particle size and zeta potential measurements (5 repetitions) of the colloidal suspension were carried out using a particle size (dynamic light scattering) and Z potential analyzer (Nanotrac Wave, Model MN401, Microtract, FL, USA).

Preparation and characterization of ^{99m}Tc -BMEDA and ^{99m}Tc -HYNIC-DA

^{99m}Tc -BMEDA. Radiolabelling was carried out according to the method used by Santos Cuevas *et al.*⁴⁵ One hundred mg of

N,N-bis(2-mercaptoethyl)-*N,N'*-diethyl-ethylenediamine BMEDA (ABX-Germany) were dissolved in 1 mL of saline solution (0.9% NaCl). Five μL of 10 fold diluted solution (50 μg , 0.224 μmol , 223.27 g mol^{-1}) was added to 25 μL of $^{99\text{m}}\text{Tc}$ -pertechnetate (GETEC-ININ-Mexico, Ocoyoacac Mex, Mexico; 740–925 MBq) followed by 7 μL of deprotection mixture (50 mg mL^{-1} sodium tartrate in 0.1 M $\text{NH}_4\text{OH}/\text{NH}_4\text{CH}_3\text{COOH}$, pH 5) and 5 μL of reducing solution (1 mg mL^{-1} SnCl_2 in 0.012 mol L^{-1} HCl). The final mixture was incubated for 20 min at room temperature. This complex was used to compare the retention times during HPLC measurements.

$^{99\text{m}}\text{Tc}$ -HYNIC-DA. Radiolabelling was carried out by adding 500 μL of EDDA-tricine solution (30 mg of EDDA in 1.5 mL of 0.1 mol L^{-1} NaOH and 60 mg of tricine in 1.5 mL of 0.2 mol L^{-1} phosphate buffer, pH = 7), 25 μL of SnCl_2 solution (1 mg mL^{-1} in 0.012 mol L^{-1} HCl), 500 μL of saline solution, and 25 μL of $^{99\text{m}}\text{Tc}$ -pertechnetate (GETEC-ININ-Mexico, Ocoyoacac Mex, Mexico; 740–925 MBq) to 200 μL HYNIC-DA (1 mg mL^{-1} in ethanol, 0.621 μmol , 321.70 g mol^{-1}), followed by incubation at 92 $^\circ\text{C}$ for 20 min in a dry block heater.

Radiochemical purity. The radiochemical purity in both cases ($^{99\text{m}}\text{Tc}$ -BMEDA and $^{99\text{m}}\text{Tc}$ -HYNIC-DA) was determined by instant thin-layer chromatography on silica gel (ITLC-SG) using saline solution as a solvent, and reversed phase HPLC on a C18 column ($\mu\text{Bondapak C18}$ column; Waters) using a Waters Empower system with an inline radioactivity detector and a gradient of water/acetonitrile containing 0.1% TFA from 95/5 (v/v) to 20/80 (v/v) over 35 min at a flow rate of 1 mL min^{-1} . Using this system, free $^{99\text{m}}\text{TcO}_4^-$ is dissolved in the solvent and moved (ITLC-SG) out in HPLC exhibiting a $t_{\text{R}} = 3\text{--}3.5$ min.

Hydrophobicity and partition coefficient (log *P*) for $^{99\text{m}}\text{Tc}$ -BMEDA and $^{99\text{m}}\text{Tc}$ -HYNIC-DA: experimental determination. 20 μL of each $^{99\text{m}}\text{Tc}$ complex was added into a mixture of equal volumes of 1-octanol and water (500 μL) and incubated overnight on a shaker. After the layer separation, 20 μL of each layer was taken and counted in a well-gamma counter. The partition coefficient was calculated as the logarithm of the quotient (counts in the 1-octanol phase)/(counts in the aqueous phase).

Liposome and HDL labeling efficiencies

10 μL of $^{99\text{m}}\text{Tc}$ -BMEDA solution (11.9 μg , 0.05 μmol) and 100 μL of $^{99\text{m}}\text{Tc}$ -HYNIC-DA solution (16 μg , 0.05 μmol) were added to liposomes (1 mL) respectively and incubated at 40 $^\circ\text{C}$ for 60 minutes. Exactly, the same procedure was employed for labeling HDL nanoparticles. The $^{99\text{m}}\text{Tc}$ -compounds were separated from free $^{99\text{m}}\text{Tc}$ -BMEDA/ $^{99\text{m}}\text{Tc}$ -HYNIC-DA using a PD-10 column eluted with normal saline solution. Each 0.5 mL fraction was collected into a tube and counted using a gamma counter. The opacity of liposomes and HDL was used to visually monitor the collection of the $^{99\text{m}}\text{Tc}$ -liposomes and $^{99\text{m}}\text{Tc}$ -rHDL respectively. The labeling efficiency was determined from the radio-chromatogram as the ratio of the counts from the liposome/HDL fractions divided by the total counts from all collected fractions.

In all cases ($^{99\text{m}}\text{Tc}$ -BMEDA-liposomes, $^{99\text{m}}\text{Tc}$ -HYNIC-DA-liposomes, $^{99\text{m}}\text{Tc}$ -BMEDA-HDL and $^{99\text{m}}\text{Tc}$ -HYNIC-DA-rHDL), the fifth fraction of the radio-chromatogram was centrifuged in a dialysis tube (MWCO of 100 000 Da) at 2500g for 15 min. The fraction representing MW less than 100 000 Da was counted using a gamma counter, and the fraction with MW higher than 100 000 Da was taken out from the tube.

In vitro stability of labeled liposomes and labeled HDL in human serum

To determine the stability of $^{99\text{m}}\text{Tc}$ -BMEDA-liposomes, $^{99\text{m}}\text{Tc}$ -HYNIC-DA-liposomes, $^{99\text{m}}\text{Tc}$ -BMEDA-rHDL, and $^{99\text{m}}\text{Tc}$ -HYNIC-DA-rHDL in serum, 150 μL of the fifth fraction eluted from the PD-10 column (most opaque fraction containing the labeled liposomes/HDL: concentration 0.33 mg mL^{-1}) was incubated at 37 $^\circ\text{C}$ with 5 mL of 5 \times diluted human serum. The radiochemical stability of the labeled liposomes/HDL was determined by taking 1 mL of the incubated particles at different time points following the addition of 300 μL of TFA for protein precipitation. Samples were centrifuged at 2000 rpm for 3 min, and the whole sample, the pellet and supernatant radioactivities were determined in a gamma counter. Pellet activity represents the activity of the labeled liposomes/HDL since liposomes and HDL are associated with the precipitated protein. Any instability in the system, recognized as a leak of the $^{99\text{m}}\text{Tc}$ -BMEDA or $^{99\text{m}}\text{Tc}$ -HYNIC-DA compounds from the liposomes/HDL, would be determined in the supernatant. Control samples were analyzed to demonstrate that neither $^{99\text{m}}\text{Tc}$ -BMEDA nor $^{99\text{m}}\text{Tc}$ -HYNIC-DA precipitates with TFA. In this case, the procedure was the same as that already described except for adding 150 μL of $^{99\text{m}}\text{Tc}$ -BMEDA or $^{99\text{m}}\text{Tc}$ -HYNIC-DA compounds to serum albumin instead of the labeled liposomes/rHDL.

Cell uptake experiments

PC3 cells were harvested and diluted in fresh medium (1×10^5 cells per well, 0.5 mL) and then seeded in 24-well tissue culture plates. After 24 h, the medium was removed, and the cells were incubated with 100 μL per well of phosphate buffered saline (PBS) with the following treatments per well: 2 kBq of $^{99\text{m}}\text{TcO}_4^-$, and 30 μL of 1 $\mu\text{g mL}^{-1}$ of $^{99\text{m}}\text{Tc}$ -rHDL, $^{99\text{m}}\text{Tc}$ -liposome, and $^{99\text{m}}\text{Tc}$ -HYNIC-DA for 45 min at 37 $^\circ\text{C}$. Then the cells were rinsed two times with 0.5 mL of ice-cold PBS. These two washes were combined and represent the $^{99\text{m}}\text{TcO}_4^-$, $^{99\text{m}}\text{Tc}$ -rHDL, $^{99\text{m}}\text{Tc}$ -liposome, and $^{99\text{m}}\text{Tc}$ -HYNIC-DA not bound to the cells. The cells were washed with 1 mL of PBS and later were incubated twice with 0.5 mL of glycine-HCl (50 mM, pH 2.8). Then glycine-HCl washes were combined, and these washes recovered the $^{99\text{m}}\text{TcO}_4^-$, $^{99\text{m}}\text{Tc}$ -rHDL, $^{99\text{m}}\text{Tc}$ -liposome, and $^{99\text{m}}\text{Tc}$ -HYNIC-DA adhered or bound to the cell membrane. The cells were washed with 1 mL of PBS, and finally were washed twice with 0.5 mL of 1.0 M NaOH (lysed cells) to recover the $^{99\text{m}}\text{TcO}_4^-$, $^{99\text{m}}\text{Tc}$ -rHDL, $^{99\text{m}}\text{Tc}$ -liposome, and $^{99\text{m}}\text{Tc}$ -HYNIC-DA internalized in the cytoplasm (washes were combined). Radioactivity was measured in the initial PBS, glycine-HCl and NaOH combined washes using a NaI(Tl) detector (NML Inc.,

USA). The initial activity of each treatment was taken to represent 100% of activity. In parallel, the nonspecific binding was determined using 30 μL of 60 $\mu\text{g } \mu\text{L}^{-1}$ of unlabeled rHDL, which blocked SR-B1 receptors on PC3 cells.

^{99m}Tc-HYNIC-DA-HDL biodistribution and imaging studies

All animal procedures were performed in accordance with the Guidelines for Care and Use of Laboratory Animals of Universidad Autónoma del Estado de México and experiments were approved by the Animal Ethics Committee of Universidad Autónoma del Estado de México. *In vivo* studies in mice were carried out according to the rules and regulations of the Official Mexican Norm 062-ZOO-1999. Normal male Balb/c mice and athymic nude mice, 6–7 weeks, were kept in sterile cages with sterile wood-shaving beds, constant temperature, humidity, noise, and 12 h light/dark cycles. Water and feed (standard PMI 5001 feed) were given *ad libitum*.

Normal mice. Normal male Balb/c mice were injected in the tail vein with ^{99m}Tc-HYNIC-DA-rHDL (200 μL , 3 MBq) under 2% isoflurane anesthesia. The mice were sacrificed at 0.5, 2, 4 and 24 h (3 mice for each time point) after radiopharmaceutical administration. Whole heart, lungs, liver, spleen, kidneys, samples of blood, intestines, bone, muscle, pancreas, and brain were transferred to pre-weighed plastic test tubes or bags. The activity was determined in a well-type scintillation detector along with two aliquots of a diluted standard representing 100% of the injected dose. The mean activities were used to obtain the percentage of injected activity per gram of tissue.

Mice bearing PC3 tumor. For tumor studies two tumor models in athymic mice (6–7 weeks) were studied. In the first one, mice were inoculated with PC3 cells subcutaneously in the upper back and in the second one, mice were inoculated with PC3 cells by injection into the tail vein. In both cases 2×10^6 PC3 cancer cells suspended in 0.1 ml PBS were used.

Subcutaneous inoculation: in the case of the subcutaneous tumor inoculation, the injection sites were observed at regular intervals for tumor formation and progression. Once the tumor was observed in the upper back of mice, mice were injected in the tail-vein or intra-tumour with ^{99m}Tc-rHDL (200 μL , 3 MBq) under 2% isoflurane anesthesia. In both cases, mice were sacrificed at 24 h ($n = 3$ for each mice) after radiopharmaceutical administration, and in the case of intra-tumoral injection they were also sacrificed after 5 min post-injection. Whole heart, lungs, liver, spleen, kidneys, tumor, samples of blood, intestines, bone, pancreas, and muscle were transferred to pre-weighed plastic test tubes. The activity was determined in a well-type scintillation detector along with two aliquots of a diluted standard representing 100% of the injected dose. The mean activities were used to obtain the percentage of injected activity per gram of tissue (%ID per g) and the percentage of injected activity per organ (%ID per organ). ^{99m}Tc-SPECT/CT imaging single photon emission computed tomography (SPECT) and X-ray computed tomography (CT) images were acquired at 4 h after the injection of ^{99m}Tc-rHDL using a micro SPECT/CT scanner (Albira, ONCOVISION; Gem

Imaging S.A., Valencia, Spain) to verify the PC3 tumor uptake. Mice under 2% isoflurane anesthesia were placed in the prone position and half body (torax) imaging was performed. The micro-SPECT field of view was 40 mm, a symmetric 20% window was set at 140 keV and multi pinhole collimators were used to acquire a 3D SPECT image with a total of 64 projections for 30 s, over 360°. The image dataset was then reconstructed using the ordered subset expectation maximization (OSEM) algorithm with standard mode parameters as provided by the manufacturer. CT parameters were 35 kV surge voltage, 700 μA current and 600 micro-CT projections.

Tail vein inoculation: after tail vein injection, it is expected that tumor grows in the pulmonary vasculature. Ten days after the tumor inoculation, mice were injected (200 μL , 3 MBq) in the tail-vein with ^{99m}Tc-rHDL and ^{99m}Tc-liposomes respectively ($n = 3$ each) under 2% isoflurane anesthesia. SPECT and radiographic computed tomography (CT) images were acquired at 0.5, 2, 4 and 24 h after radiopharmaceutical injection using a micro-SPECT/CT scanner (Albira, ONCOVISION; Gem Imaging S.A., Valencia, Spain) under the same conditions described above. From the radiopharmaceuticals ^{99m}Tc-rHDL and ^{99m}Tc-liposomes injected doses, and the weight of each mouse, the mean standardized uptake value in the tumor (SUV mean) was calculated using PMOD Data Analysis Software (PMOD Technologies).

Radiokinetic ^{99m}Tc-HYNIC-DA-HDL

From the percentages of injected dose per organ (%ID per organ) at different times in the main target organs (determined from the biodistribution), the $A_h(t)$ functions were obtained ($A_h(t) = q_h(t)e^{-(\lambda_B + \lambda_R)t}$) and the total number of disintegrations $N(\text{MBq h/MBq})$ of ^{99m}Tc in the organ normalized to unit-administered activity was also calculated. The $A_h(t)$ functions and total number of disintegrations $N(\text{MBq h/MBq})$ in the tumor were also calculated for ^{99m}Tc-rHDL and ^{99m}Tc-liposome administrations.

Results and discussion

The combination of HYNIC and the ethylenediamine-*N,N'*-diacetic acid (EDDA) with tricine has been successfully employed as a bi-functional chelator for labeling peptides and gold nanoparticles with ^{99m}Tc due to its high stability with the HYNIC imine bond. The EDDA/tricine completes the coordination sphere of the ^{99m}Tc complex.^{46–48} This ^{99m}Tc-HYNIC/EDDA/tricine complex is suitable for *in vivo* studies as it facilitates urinary excretion (hydrophilic properties) of the isotope. However, a hydrophilic compound would not be efficiently encapsulated into the core of the rHDL unless it is modified to have hydrophobic properties as described herein. Specifically, HYNIC-DA was synthesized as a lipophilic derivative of HYNIC (see the Materials and methods section) to facilitate the incorporation of a bi-functional chelator-complexed ^{99m}Tc into liposomes and rHDL nanoparticles. Fig. 1 shows the synthetic

scheme for HYNIC-DA as well as state-of-the-art of ^{99m}Tc coordination chemistry⁴⁹

Liposome and HDL characterization

Data on the characterization of liposomes and HDL are shown in Table 1. As can be seen, the liposomal NPs are much larger than the rHDL NPs, while both were found to be very stable (colloidal stability) in suspension, as indicated by their respective Z-potentials. Both nanoparticles had an acceptable homogeneity as indicated by the observed polydispersity index values.

Preparation of ^{99m}Tc -BMEDA and ^{99m}Tc -HYNIC-DA

The method used in this work for the labeling of BMEDA with ^{99m}Tc was different compared to the conventional glutathione encapsulated liposome method.⁵⁰ In the conventional approach, the liposome is pre-loaded with reduced glutathione (GSH), and ^{99m}Tc is complexed with BMEDA through ^{99m}Tc -glucoheptonate in three steps: (i) uploading liposomes with GSH, (ii) preparing the ^{99m}Tc -glucoheptonate from $^{99m}\text{TcO}_4^-$, and (iii) preparing the ^{99m}Tc -BMEDA complex (^{99m}Tc -“SNS/S” type of complex). The labeling efficiency of this method is usually limited (below 85%). During these studies, the liposomes were not employed for BMEDA labeling with ^{99m}Tc . Instead the ^{99m}Tc -BMEDA was prepared in a single step using the same methodology reported earlier⁵¹ to prepare a ^{99m}Tc - N_2S_2 complex. This method facilitates a simpler and more efficient labeling procedure. The radiochemical purity of the product determined by ITLC-SG and HPLC was 90–95%.

The ^{99m}Tc -labeling of HYNIC-DA was also carried out in one step, following the methodology already reported to form the ^{99m}Tc -HYNIC complex.⁴⁵ As with the ^{99m}Tc -BMEDA, the radiochemical purity determined by ITLC-SG and HPLC was within 90–95%.

Hydrophobicity and partition coefficient ($\log P$) for ^{99m}Tc -BMEDA and ^{99m}Tc -DA-HYNIC

Hydrophobicity is directly proportional to the retention time of RP-HPLC, as previously reported.⁵² Fig. 2 shows the RP-HPLC radio-chromatogram of ^{99m}Tc -HYNIC-DA and ^{99m}Tc -BMEDA. These data show that ^{99m}Tc -HYNIC had a higher retention time (1.73 min higher) than ^{99m}Tc -BMEDA, indicating that it is more hydrophobic. These findings agree with the experimental partition coefficient determined for these compounds, -1.30 for ^{99m}Tc -BMEDA and 0.25 for ^{99m}Tc -HYNIC-DA (the real complex is ^{99m}Tc -HYNIC-DA/EDDA, since HYNIC

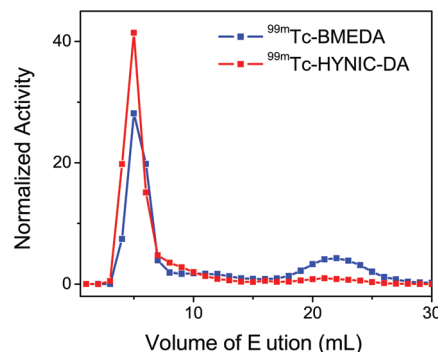


Fig. 2 Labelling efficiency of HDL fractions collected at different elution times.

cannot complete the coordination sphere of ^{99m}Tc and EDDA is therefore used for this purpose). The negative value for ^{99m}Tc -BMEDA and the positive value for ^{99m}Tc -HYNIC indicate that ^{99m}Tc -HYNIC-DA is more hydrophobic than ^{99m}Tc -BMEDA, and the difference in hydrophobicity is slightly over one log unit. When estimated by the method built into the Chem3D molecular modeling software, the $\log P$ for BMEDA was found to be 1.54, while for HYNIC-DA it was 3.85. The hydrophobicity of these molecules is reduced with the formation of the metal complexes, but the trend is maintained in that HYNIC-DA molecule, which is more hydrophobic than BMEDA; *i.e.* ^{99m}Tc -HYNIC-DA remains more hydrophobic than ^{99m}Tc -BMEDA as expected. From these findings, it is anticipated that ^{99m}Tc -HYNIC-DA can be incorporated into the hydrophobic layer of liposomes and into the hydrophobic core of HDL more efficiently than ^{99m}Tc -BMEDA.

Liposome and HDL labeling efficiencies

Fig. 3 shows the labeling efficiency of rHDL with ^{99m}Tc -BMEDA and ^{99m}Tc -HYNIC-DA respectively. For both nanoparticles, the labeling efficiency is always higher with ^{99m}Tc -HYNIC-DA than ^{99m}Tc -BMEDA. For liposomes, yields were $(66 \pm 2)\%$ vs. $(61 \pm 2)\%$ respectively while for rHDL yields were $(86 \pm 3)\%$ vs. $(57 \pm 3)\%$. For both ^{99m}Tc -complexes,

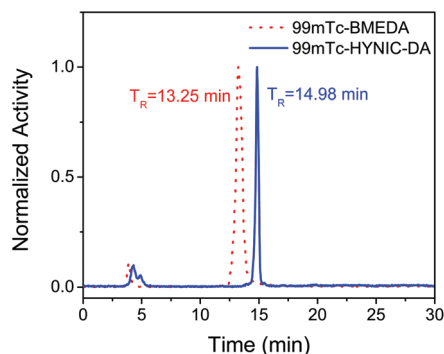


Fig. 3 RP-HPLC radio-chromatogram of ^{99m}Tc -BMEDA and ^{99m}Tc -HYNIC-DA complexes.

Table 1 Characterization of the liposome and HDL nanoparticles

Parameter	Liposomes	rHDL
Particle diameter (nm)	107.4 ± 15	36.60 ± 10
Polydispersity	0.186 ± 0.04	0.28 ± 0.05
Z-Potential (mV)	-18.15 ± 6	-20.60 ± 7
Phospholipid (mg mL^{-1})	23.34 ± 4	1.55 ± 0.6
Protein (mg mL^{-1})	N/A	1.19 ± 0.3

the labeling efficiency of rHDL was always higher than that of the liposomes. These differences are explained by the relative hydrophobicities of these ^{99m}Tc -conjugates (^{99m}Tc -HYNIC-DA is more hydrophobic).

Schematically, the labeled HDL with ^{99m}Tc -HYNIC-DA can be represented as shown in Fig. 4 (^{99m}Tc -rHDL). The blue spheres represent the phospholipids and cholesterol forming the outer region; the orange diamonds represent the ^{99m}Tc -complex (^{99m}Tc -BMEDA or ^{99m}Tc -HYNIC-DA) while the tail of the DA molecule is buried in the core of the particle. The green cylinders represent the amphipathic peptide chain of the Apo A-1 protein stabilizing the spherical structure of rHDL nanoparticles making it water soluble.

^{99m}Tc -BMEDA is the conventional labeling agent for liposomes, but usually, liposomes are loaded with glutathione (GSH) in the inner core, so once the ^{99m}Tc -BMEDA passes through the hydrophobic outer shell it reaches the hydrophilic core and there ^{99m}Tc -BMEDA is reduced by GSH becoming more hydrophilic and entrapped in the central core.⁵⁰ During these studies, the liposomes were not loaded with GSH; therefore both ^{99m}Tc -BMEDA and ^{99m}Tc -HYNIC-DA remained in the outer hydrophobic shell of liposomes. Finally, the lipid layer of HDL is hydrophobic; therefore, ^{99m}Tc -complexes are loaded inside the NP *via* the HYNIC-DA conjugate (Fig. 4). Because ^{99m}Tc -HYNIC-DA is more hydrophobic (larger $\log P$ and retention time in RP-HPLC), it has a larger distribution in hydrophobic areas than ^{99m}Tc -BMEDA, that facilitates higher labeling efficiency.

As seen in Fig. 3, the labeled compounds eluted in the same volume and the fraction in both cases (*i.e.*, both labeling liposomes and rHDL). These fractions were visibly cloudy, facilitating their visual detection. In order to assure that the radioactivity in the NP fractions is due to the internalization of the ^{99m}Tc -complex into the nanoparticles and not due to the co-elution of aggregated or free compound with the NPs, the most radioactive fraction (which was also the cloudiest) was centrifuged using a centrifugation tube containing a dialysis membrane of MWCO of 100 000 Da. All the radioactivity was found inside the membrane, meaning that no aggregation of ^{99m}Tc -complexes was present (any ^{99m}Tc -complex aggregation would have a molecular weight of less than 100 000 Da). This confirms that the ^{99m}Tc -complexes were associated with the rHDL NPs.

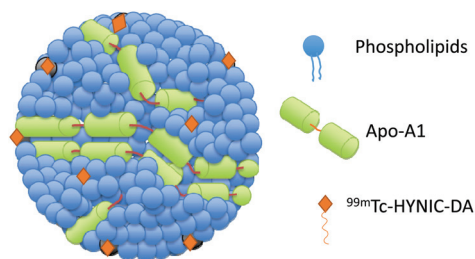


Fig. 4 Schematic structure of the labeled rHDL with the localization of HYNIC-DA.

In vitro stability of labeled liposomes and labeled HDL in human serum

Stability is understood as the capacity of ^{99m}Tc -BMEDA and ^{99m}Tc -HYNIC-DA for remaining entrapped into the HDL without leaking. The results presented in Table 2 are in agreement with those reported in earlier sections. The lower hydrophobicity of ^{99m}Tc -BMEDA in comparison to ^{99m}Tc -HYNIC-DA explains the higher stability and retention of ^{99m}Tc -HYNIC-DA into the nanoparticles. After 3 h of incubation, more than 90% of ^{99m}Tc -HYNIC-DA is still inside the liposomes and HDL. Due to lower stability of the BMEDA, it was not used in the animal studies.

In vitro cell uptake study

All of the radioactivity uptake by the cell was found in the cytoplasm when the rHDL NPs were used to deliver the radio-imaging agent. Moreover, a partial blocking of the SR-B1 receptor with increasing concentrations of empty rHDL as the competitive inhibitor markedly decreased the total uptake of the labeled rHDL by about 60% (the remainder ascribed to membranous accumulation; data not shown). Liposome delivery did not change with HDL blocking as the method of internalization of liposomal radioisotope is independent of SR-B1 expression and hence no change was observed (ESI Fig. S1†). The other two groups, ^{99m}Tc -HYNIC-DA and $^{99m}\text{TcO}_4^-$ salt, were used as controls resulting in only marginal incorporation into the cells (data not shown).

Fig. S1† shows no significant difference in the liposome cell uptake in the presence and absence of unlabeled rHDL (SR-B1 blocking agent). The internalization of the liposome into the cell is through an endocytic mechanism which is different from the SR-B1 mediated non-endocytic delivery. The uptake of liposomes by the cell membrane is anticipated to be due mostly to its adsorption on the cell membrane. Liposomal uptake, therefore, is non-specific. A similar approach of using liposomes as a negative control of HDL was also employed by Murphy *et al.* where they demonstrated that HDL inhibited the activity of CD11b while liposomes did not.⁵³ The results in Fig. 5 agree with the findings reported by Mooberry *et al.*⁵⁴ Moreover, several others have reported the specific recognition of HDL by the SR-B1 receptor by labeling HDL with ^3H or ^{14}C and blocking the receptor using un-labeled rHDL.^{55–57}

Although ^{99m}Tc -HYNIC-DA and $^{99m}\text{TcO}_4^-$ are not expected to be found in the solution of ^{99m}Tc -rHDL as separate species, as it was already purified, and ^{99m}Tc -HYNIC is stable inside

Table 2 Results of the *in vitro* stability test for liposomes and rHDL nanoparticles in human serum

Time (h)	^{99m}Tc -BMEDA-liposomes	^{99m}Tc -HYNIC-DA-liposome	^{99m}Tc -BMEDA-rHDL	^{99m}Tc -HYNIC-DA-rHDL
1	92 ± 5	98 ± 2	100	100
2	80 ± 3	95 ± 1	87 ± 5	100
3	73 ± 6	91 ± 3	78 ± 2	96.5 ± 0.6

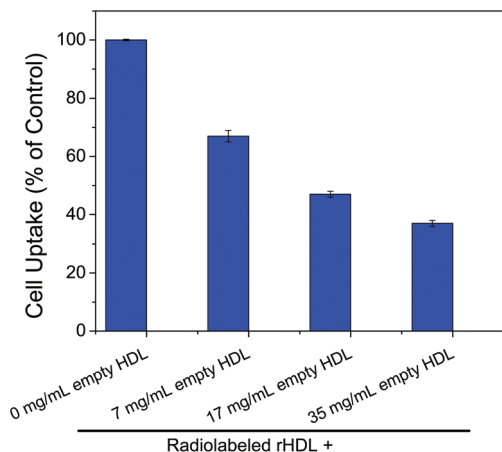


Fig. 5 *In vitro* cell uptake experiment with and without the blocking agent.

the rHDL, their uptake by PC-3 cells was studied as controls. ^{99m}Tc -HYNIC-DA showed a total uptake of 34% and 31% without and with SR-B1 blocking respectively. On the other hand, $^{99m}\text{TcO}_4^-$ was found to have a total uptake of 2.9% and 2.8% with and without SR-B1 blocking respectively. These results show as expected that the uptake of these formulations is very low and nonspecific.

^{99m}Tc -DA-HYNIC-HDL biodistribution and imaging studies

^{99m}Tc -HYNIC-DA-rHDL showed better stability than ^{99m}Tc -BMEDA-HDL, and for this reason, the bio-distribution and imaging studies were only carried out with the ^{99m}Tc -HYNIC-DA-rHDL.

Although ^{99m}Tc -HYNIC-DA-liposome also showed good stability, the bio-distribution of these nanoparticles was not studied because liposome bio-distribution has already been studied.^{58–60} However, this is the first time that HDL type NPs have been labeled with ^{99m}Tc , therefore studies of their bio-distribution in normal mice at different times post-injection were carried out (Table 3).

Table 3 confirms the delivery and hepatobiliary excretion pattern of the ^{99m}Tc -HYNIC-DA-rHDL NPs. In normal animals rHDL NPs were expected to accumulate in liver tissue, due to its high SR-B1 expression. Hence the increased liver uptake was observed with post 0.5 h time points. These data confirm the passive targeting of the SR-B1 receptors showing a higher concentration of the radio-imaging agent in the liver. Other organs such as spleen, lungs, and kidney showed moderate radioactivity while heart and pancreas exhibited very low radioactivity, due to the established absence of SR-B1 receptors. This observation is particularly important in establishing the targeting potential and limiting the off-target bio-distribution of the payload transported by the rHDL NPs.

Moreover, a similar study in tumor-bearing mice was conducted to evaluate tumor uptake as a function of time. Table 4 shows the Standard Uptake Values (SUV) for the ^{99m}Tc -rHDL and ^{99m}Tc -liposomes. In the case of rHDL the SUV value

Table 3 Biodistribution of ^{99m}Tc -rHDL in normal male balb/C mice

Organs	% (Injected activity)/(g of tissue)			
	Time post-injection			
	0.5 h	2.0 h	4.0 h	24 h
Blood	1.55 ± 0.07	0.57 ± 0.08	0.31 ± 0.08	0.19 ± 0.10
Heart	2.64 ± 2.50	0.75 ± 0.30	0.47 ± 0.27	0.39 ± 0.36
Spleen	7.91 ± 0.70	19.01 ± 10.33	9.78 ± 3.43	23.82 ± 4.16
Intestine	1.41 ± 1.31	2.72 ± 2.45	1.42 ± 1.57	0.21 ± 0.12
Pancreas	2.18 ± 1.60	1.98 ± 2.07	1.06 ± 0.98	0.62 ± 0.51
Kidney	5.12 ± 3.77	2.55 ± 1.27	1.49 ± 0.14	0.58 ± 0.13
Liver	36.23 ± 19.45	23.55 ± 1.04	20.56 ± 7.54	20.66 ± 6.26
Lungs	23.34 ± 10.69	9.64 ± 6.49	7.71 ± 2.00	1.95 ± 1.80
Muscle	1.53 ± 1.07	0.50 ± 0.30	0.25 ± 0.06	0.31 ± 0.36
Bone	3.42 ± 2.87	1.02 ± 0.84	2.21 ± 1.10	1.17 ± 0.84
Brain	0.56 ± 0.53	0.29 ± 0.34	0.10 ± 0.07	0.04 ± 0.02

Table 4 Standard uptake values (SUV mean) of PC3 tumors induced in athymic balb/c mice by tail vein inoculation

Time (h)	^{99m}Tc -rHDL tumor uptake (SUV mean)	^{99m}Tc -liposome tumor uptake (SUV mean)
0.5	0.200 ± 0.061	0.147 ± 0.048
2.0	0.312 ± 0.056	0.198 ± 0.051
4.0	1.513 ± 0.038	0.174 ± 0.047
24.0	2.800 ± 0.021	0.037 ± 0.023

increased more than 10 fold in 24 h while these values remained constant for liposomal preparation during the first few hours, and decreased after 4 h as evident from the data. The SR-B1 expression on PC3 tumor cells thus attracts the rHDL NPs leading to higher accumulation of ^{99m}Tc .

Table 5 shows the bio-distributions after 5 min and 24 h following intra-tumoral injections, as well as the bio-distributions after 24 h of intravenous injection of ^{99m}Tc -HYNIC-DA-rHDL in mice bearing subcutaneous PC3 tumors. The tumor/organ

Table 5 Biodistribution of mice bearing PC3 tumors after intra-tumoral and intravenous injections

Organ	% (Injected activity)/(g of tissue)		Tumor/organ ratio	
	5 min, intra-tumoral injection	24 h, intra-tumoral injection	24 h, intravenous injection	24 h, intravenous injection
Blood	0.11 ± 0.10	0.31 ± 0.15	0.16 ± 0.09	37 ^a
Heart	2.50 ± 0.98	0.06 ± 0.07	0.60 ± 0.31	7.6
Spleen	0.20 ± 0.14	0.73 ± 0.62	16.03 ± 5.8	0.4
Intestine	0.24 ± 0.19	0.01 ± 0.02	0.51 ± 0.36	4
Pancreas	0.21 ± 0.08	0.15 ± 0.11	2.51 ± 1.1	2.7
Kidney	0.78 ± 0.47	0.53 ± 0.25	1.29 ± 0.63	2.5
Liver	1.16 ± 0.41	1.13 ± 0.61	32.14 ± 8.6	0.01
Lungs	6.32 ± 2.1	0.01 ± 0.03	1.81 ± 1.51	3.6
Muscle	0.28 ± 0.10	0.41 ± 0.19	1.51 ± 0.39	3.87
Bone	0.14 ± 0.09	0.19 ± 0.11	1.12 ± 1.01	5.7
Tumor	88.50 ± 3.24	30.75 ± 5.32	5.96 ± 2.03	1

^a Ratio calculated as %IA per g(tumor)/%IA per g(blood).

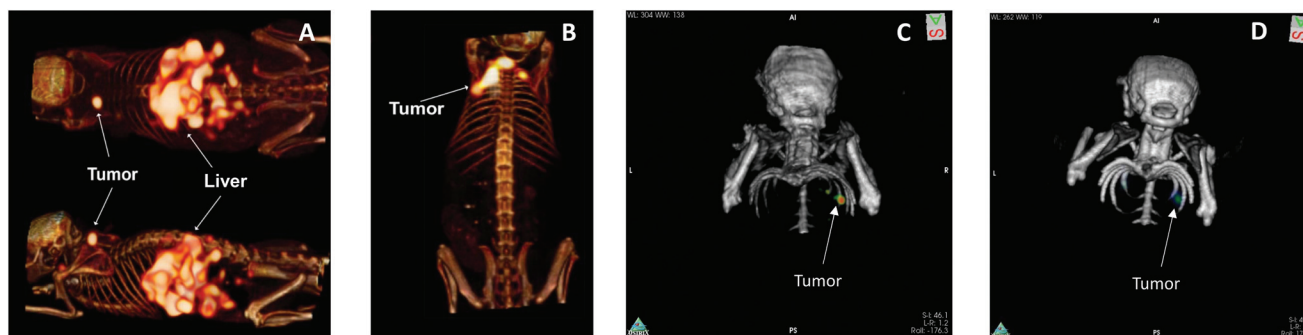


Fig. 6 SPECT/CT images after 4 h of post injection of ^{99m}Tc -rHDL in athymic mice bearing PC3 tumors induced subcutaneously, (A) intravenous injection and (B) intra-tumoral injection. SPECT/CT images after 4 h of post injection intravenously in athymic mice bearing PC3 tumors induced by tail vein inoculation, (C) ^{99m}Tc -rHDL and (D) ^{99m}Tc -liposomes.

ratio after 24 h of intravenous injection is also shown. Liver, spleen and tumor showed a significantly higher activity after intravenous injection suggesting efficient targeting to tumor tissue. In fact, tumor tissue radioactivity was substantially higher compared to heart, blood, intestine, pancreas, kidney, lungs, muscles, and bones. This is especially important for the delivery of chemotherapy drugs such as doxorubicin where cardiotoxicity is a major concern. In the case of the heart, the amount received was ten-fold less compared to tumor tissue at 24 h.

Fig. 6 shows the SPECT/CT images after four hours following intravenous (Fig. 6A) and intra-tumoral injection (Fig. 6B) respectively in mice bearing a PC3 tumor. As expected, radioactivity is accumulated in the PC3 tumor, due to the over-expression of SR-B1 receptors that mediate the internalization of the rHDL payload (^{99m}Tc -HYNIC-DA). The high accumulation of ^{99m}Tc -rHDL in the liver is consistent with the bio-distribution results shown in Table 5. Fig. 6C and D show the SPECT/CT images after 4 h of intravenous injection in mice bearing a PC3 tumor induced by tail-vein inoculation. It was expected that PC3 cancer cells tend to harbor in the lungs predominantly. Thus, we see a higher uptake in these cells in lung tissue where PC3 cells are lodged. Images correlate with the SUV mean values reported in Table 4 and also highlight the receptor-specific uptake of rHDL nanoparticles. Additional time-course images of radiolabeled rHDL are shown in ESI Fig. S2.†

^{99m}Tc -HYNIC-DA-rHDL radiokinetic model

ESI Table S1† shows the radiokinetic model and the total disintegrations occurred in the excretory organs and tumor after the administration of ^{99m}Tc -HYNIC-DA-rHDL. The long residence time of total disintegrations of ^{99m}Tc -rHDL in the tumor, which is 15 times higher than the ^{99m}Tc -liposomes, is noteworthy. Although we are aware of the preferable non-endocytic delivery of payloads from the rHDL NPs, we are not certain regarding the exact delivery mechanism that facilitated the enhanced tumor accumulation and retention of ^{99m}Tc as these types of studies are beyond the scope of the current investigation. Perhaps, these find-

ings may be ascribed to efficient targeting *via* SR-B1 and the lack of a well-developed venous structure in the tumor mass that may facilitate the extended retention of ^{99m}Tc -DA at the tumor site. The substantially extended retention time of ^{99m}Tc -rHDL justifies its use in tumor imaging, and also suggests an effective therapeutic application for the rHDL platform; therefore, these NPs could be most useful for the development of theranostic radio-nanopharmaceuticals.

Conclusions

6-Hydrazinopyridine-3-carboxylic acid dodecylamide (HYNIC-DA) was synthesized and labeled with a ^{99m}Tc nuclide, achieving high radiochemical purity. The ^{99m}Tc -complex is more hydrophobic than conventional ^{99m}Tc -BMEDA, perhaps resulting in 90% of ^{99m}Tc -HYNIC-DA remaining entrapped into liposomes and rHDL after three hours of incubation. Therefore, ^{99m}Tc -HYNIC-DA is a good alternative to label amphiphilic nanoparticles such as rHDL and liposomes with adequate efficiency and stability. Bio-distribution and imaging studies carried out with mice carrying PC3 tumors showed high radioactivity uptake in the tumor and the liver apparently due to the SR-B1 targeting and subsequent payload accumulation. Findings from *in vivo* studies are consistent with those from *in vitro* cell uptake studies where the specific recognition of ^{99m}Tc -rHDL was demonstrated by SR-B1 blockade with unlabeled rHDL and control experiment with ^{99m}Tc -liposome evaluated the nonspecific uptake. Determination of SUVs also agrees with cell uptake experiments, showing higher values with ^{99m}Tc -rHDL compared to ^{99m}Tc -liposomes (steady and lower SVU mean values). This nanosystem (^{99m}Tc -rHDL) shows favorable properties that warrant consideration as a radiopharmaceutical for the diagnosis of cancers, especially those exhibiting overexpressed SR-B1 receptors. Combining the drug delivery capabilities of rHDL as well as its potential as a radiopharmaceutical transporter for diagnosis, rHDL NPs may also be utilized in the design of a broad range of new theranostic radiopharmaceuticals.

Author contributions

KIO, BOG, LAL, CLS, NPJ, MAL, LAM, BN, and NS have all conducted experiments. KIO, SR, LP, and AL have contributed to designing experiments, analysing the data, writing and revising this manuscript.

Conflicts of interest

There are no conflicts to declare.

Acknowledgements

This work was supported by the Universidad Autónoma del Estado de México (UAEMex) and the University of North Texas Health Science Center (UNTHSC) through the joined “Seed-Grant” 3889/2015FS, Wheels for Wellness, Fort Worth, and the Robert A. Welch Foundation (endowment BK-0031 to L. P.). The authors thank Samantha M. Brewer and Professor Kayla N. Green (Texas Christian University, Fort Worth) for their help in the interpretation of the NMR spectra. This research was carried out as a part of the activities of the “Laboratorio Nacional de Investigación y Desarrollo de Radiofármacos”, CONACYT-Mexico and it was also supported by the Research Sectoral Fund for Education SEP-CONACYT-Mexico through the grant number CB-2016-287217. This work was supported in part by grants from Leukemia Texas and Texas Alzheimer’s Research Care and Consortium (2018-48-51-JI) to Sangram Raut.

Notes and references

- 1 Z. Cheng, A. Al Zaki, J. Z. Hui, V. R. Muzykantov and A. Tsourkas, *Science*, 2012, **338**, 903–910, DOI: 10.1126/science.1226338.
- 2 G. Bao, S. Mitragotri and S. Tong, *Annu. Rev. Biomed. Eng.*, 2013, **15**, 253–282.
- 3 J. V. Jokerst and S. S. Gambhir, *Acc. Chem. Res.*, 2011, **44**, 1050–1060.
- 4 P. Debbage and W. Jaschke, *Histochem. Cell Biol.*, 2008, **130**, 845–875.
- 5 T. O. Munnink, W. Nagengast, A. Brouwers, C. Schröder, G. Hospers, M. Lub-de Hooge, E. van der Waals, P. Van Diest and E. De Vries, *Breast*, 2009, **18**, S66–S73.
- 6 H. Hricak, P. L. Choyke, S. C. Eberhardt, S. A. Leibel and P. T. Scardino, *Radiology*, 2007, **243**, 28–53.
- 7 W. J. Mulder, G. J. Strijkers, G. A. van Tilborg, A. W. Griffioen and K. Nicolay, *NMR Biomed.*, 2006, **19**, 142–164.
- 8 A. M. Lees, R. S. Lees, F. J. Schoen, J. L. Isaacsohn, A. J. Fischman, K. A. McKusick and H. W. Strauss, *Arteriosclerosis*, 1988, **8**, 461–470.
- 9 J. C. Frias, M. J. Lipinski, S. E. Lipinski and M. T. Albelda, *Contrast Media Mol. Imaging*, 2007, **2**, 16–23.
- 10 M. Mangaraj, R. Nanda and S. Panda, *Indian J. Clin. Biochem.*, 2016, **31**, 253–259.
- 11 J. B. Simonsen, *Nanomedicine*, 2016, **12**, 2161–2179.
- 12 A. G. Lacko, M. Nair, S. Paranjape, L. Mooberry and W. J. McConathy, *Chemotherapy*, 2006, **52**, 171–173, DOI: 10.1159/000093268.
- 13 A. G. Lacko, N. A. Sabnis, B. Nagarajan and W. J. McConathy, *Front. Pharmacol.*, 2015, **6**, 247, DOI: 10.3389/fphar.2015.00247.
- 14 Q. Lin, J. Chen, K. K. Ng, W. Cao, Z. Zhang and G. Zheng, *Pharm. Res.*, 2014, **31**, 1438–1449.
- 15 S. Acton, A. Rigotti, K. T. Landschulz, S. Xu, H. H. Hobbs and M. Krieger, *Science*, 1996, **271**(5248), 518–520.
- 16 R. Kuai, D. Li, Y. E. Chen, J. J. Moon and A. Schwendeman, *ACS Nano*, 2016, **10**(3), 3015–3041.
- 17 N. Sabnis, S. Pratap, P. Bowman, I. Akopova and A. G. Lacko, *Front. Pediatr.*, 2013, **1**, 6.
- 18 N. Sabnis, M. Nair, M. Israel, W. J. McConathy and A. G. Lacko, *Int. J. Nanomed.*, 2012, **7**, 975–983, DOI: 10.2147/IJN.S28029.
- 19 S. Yang, M. G. Damiano, H. Zhang, S. Tripathy, A. J. Luthi, J. S. Rink, A. V. Ugolkov, A. T. Singh, S. S. Dave, L. I. Gordon and C. S. Thaxton, *Proc. Natl. Acad. Sci. U. S. A.*, 2013, **110**, 2511–2516, DOI: 10.1073/pnas.1213657110.
- 20 P. M. Cruz, H. Mo, W. J. McConathy, N. Sabnis and A. G. Lacko, *Front. Pharmacol.*, 2013, **4**, 119, DOI: 10.3389/fphar.2013.00119.
- 21 A. Fiorenza, A. Branchi and D. Sommariva, *Int. J. Clin. Lab. Res.*, 2000, **30**, 141–145.
- 22 J. L. Gutierrez-Pajares, C. B. Hassen, S. Chevalier and P. G. Frank, *Front. Pharmacol.*, 2016, **7**, 338.
- 23 E. Kökoğlu, I. Karaarslan, H. M. Karaarslan and H. Baloğlu, *Cancer Lett.*, 1994, **82**, 175–178.
- 24 V. Michalaki, G. Koutroulis, K. Syrigos, C. Piperi and A. Kalofoutis, *Mol. Cell. Biochem.*, 2005, **268**, 19–24.
- 25 F. D. Shah, S. N. Shukla, P. M. Shah, H. R. Patel and P. S. Patel, *Integr. Cancer Ther.*, 2008, **7**, 33–41.
- 26 P. M. Cruz, H. Mo, W. McConathy, N. A. Sabnis and A. G. Lacko, *Front. Pharmacol.*, 2013, **4**, 119.
- 27 M. M. Shahzad, L. S. Mangala, H. D. Han, C. Lu, J. Bottsford-Miller, M. Nishimura, E. M. Mora, J. Lee, R. L. Stone and C. V. Pecot, *Neoplasia*, 2011, **13**, 309IN3–319IN8.
- 28 Z. Zhang, J. Chen, L. Ding, H. Jin, J. F. Lovell, I. R. Corbin, W. Cao, P. Lo, M. Yang and M. Tsao, *Small*, 2010, **6**, 430–437.
- 29 P. Khumsupan, R. Ramirez, D. Khumsupan and V. Narayanaswami, *Biochim. Biophys. Acta, Biomembr.*, 2011, **1808**, 352–359.
- 30 L. Cui, Q. Lin, W. Jiang, L. Ding, J. Chen and G. Zheng, Porphyrin-lipid assembled HDL-like nanovesicles for fluorescence imaging and PDT treatment of orthotopic brain glioma tumor, 2014, BT3A.55.
- 31 D. P. Cormode, T. Skajaa, M. M. van Schooneveld, R. Koole, P. Jarzyna, M. E. Lobatto, C. Calcagno, A. Barazza, R. E. Gordon and P. Zanzonico, *Nano Lett.*, 2008, **8**, 3715–3723.

- 32 C. Perez-Medina, T. Binderup, M. Lobatto, S. Baxter, C. Calcagno, S. Ishino, T. Reiner, J. Lewis, Z. Fayad and W. Mulder, *J. Nucl. Med.*, 2016, **57**, 63–63.
- 33 C. Perez-Medina, J. Tang, D. Abdel-Atti, B. Hogstad, M. Merad, E. A. Fisher, Z. A. Fayad, J. S. Lewis, W. J. Mulder and T. Reiner, *J. Nucl. Med.*, 2015, **56**, 1272–1277, DOI: 10.2967/jnumed.115.158956.
- 34 H. Sinzinger, H. Bergmann, J. Kaliman and P. Angelberger, *Eur. J. Nucl. Med. Mol. Imaging*, 1986, **12**, 291–292.
- 35 S. Ishino, T. Mukai, Y. Kuge, N. Kume, M. Ogawa, N. Takai, J. Kamihashi, M. Shiomi, M. Minami, T. Kita and H. Saji, *J. Nucl. Med.*, 2008, **49**, 1677–1685, DOI: 10.2967/jnumed.107.049536.
- 36 D. P. Cormode, J. C. Frias, Y. Ma, W. Chen, T. Skajaa, K. Briley-Saebo, A. Barazza, K. J. Williams, W. J. Mulder and Z. A. Fayad, *Clin. Lipidol.*, 2009, **4**, 493–500.
- 37 E. Lim, T. Kim, S. Paik, S. Haam, Y. Huh and K. Lee, *Chem. Rev.*, 2014, **77**, 7826–7831.
- 38 H. Huang and J. F. Lovell, *Adv. Funct. Mater.*, 2017, **50**, 533–537.
- 39 A. Fernandez-Fernandez, R. Manchanda and A. J. McGoron, *Appl. Biochem. Biotechnol.*, 2011, **165**(7–8), 1628–1651.
- 40 C. N. McEwen, R. G. McKay and B. S. Larsen, *Anal. Chem.*, 2005, **77**, 7826–7831.
- 41 S. Szarka and L. Prokai, *J. Mass Spectrom.*, 2015, **50**, 533–537.
- 42 A. Toro-Córdova, F. Ledezma-Gallegos, L. Mondragon-Fuentes, R. Jurado, L. A. Medina, J. M. Pérez-Rojas and P. Garcia-Lopez, *J. Chromatogr. Sci.*, 2016, **54**, 1016–1021.
- 43 F. Szoka Jr. and D. Papahadjopoulos, *Proc. Natl. Acad. Sci. U. S. A.*, 1978, **75**, 4194–4198.
- 44 J. C. M. Stewart, *Anal. Biochem.*, 1980, **104**, 10–14.
- 45 C. L. Santos-Cuevas, G. Ferro-Flores, C. A. de Murphy, F. d. M. Ramírez, M. A. Luna-Gutiérrez, M. Pedraza-López, R. García-Becerra and D. Ordaz-Rosado, *Int. J. Pharm.*, 2009, **375**, 75–83.
- 46 G. Ferro-Flores, C. Arteaga de Murphy, J. Rodriguez-Cortes, M. Pedraza-Lopez and M. T. Ramirez-Iglesias, *Nucl. Med. Commun.*, 2006, **251**, 7–13, DOI: 10.1097/01.mnm.0000202863.52046.7f.
- 47 B. E. Ocampo-García, F. d. M. Ramírez, G. Ferro-Flores, L. M. De León-Rodríguez, C. L. Santos-Cuevas, E. Morales-Avila, C. A. de Murphy, M. Pedraza-López, L. A. Medina and M. A. Camacho-López, *Nucl. Med. Biol.*, 2011, **38**, 1–11.
- 48 E. Morales-Avila, G. Ferro-Flores, B. E. Ocampo-García, L. M. De León-Rodríguez, C. L. Santos-Cuevas, R. García-Becerra, L. A. Medina and L. Gómez-Oliván, *Bioconjugate Chem.*, 2011, **22**, 913–922.
- 49 Technical Report Series No 466, International Atomic Energy Agency, Vienna, 2008, pp. 7–26.
- 50 A. Bao, B. Goins, R. Klipper, G. Negrete, M. Mahindaratne and W. T. Phillips, *J. Pharm. Sci.*, 2003, **92**, 1893–1904.
- 51 C. L. Santos-Cuevas, G. Ferro-Flores, C. A. de Murphy and P. A. Pichardo-Romero, *Nucl. Med. Commun.*, 2008, **29**, 741–747.
- 52 G. Ferro-Flores, F. Ramírez, M. Martinez-Mendoza, C. Murphy, M. Pedraza-Lopez and L. Garcia-Salinas, *J. Radioanal. Nucl.*, 2002, **251**, 7–13.
- 53 A. J. Murphy, K. J. Woollard, A. Hoang, N. Mukhamedova, R. A. Stirzaker, S. P. McCormick, A. T. Remaley, D. Sviridov and J. Chin-Dusting, *Arterioscler., Thromb., Vasc. Biol.*, 2008, **28**(11), 2071–2077.
- 54 L. K. Mooberry, M. Nair, S. Paranjape, W. J. McConathy and A. G. Lacko, *J. Drug Targeting*, 2010, **18**(1), 53–58.
- 55 T. A. Pagler, S. Rhode, A. Neuhofer, H. Laggner, W. Strobl, C. Hinterdorfer, I. Volf, M. Pavelka, E. R. Eckhardt, D. R. van der Westhuyzen, G. J. Schutz and H. Stangl, *J. Biol. Chem.*, 2006, **281**(16), 11193–11204, DOI: 10.1074/jbc.M510261200.
- 56 M. A. Connelly, *Mol. Cell. Endocrinol.*, 2009, **300**(1–2), 83–88, DOI: 10.1016/j.mce.2008.09.011.
- 57 M. C. de Beer, L. W. Castellani, L. Cai, A. J. Stromberg, F. C. de Beer and D. R. van der Westhuyzen, *J. Lipid Res.*, 2004, **45**(4), 706–715, DOI: 10.1194/jlr.M300417-JLR200.
- 58 E. T. M. Dams, W. J. Oyen, O. C. Boerman and G. Storm, *J. Nucl. Med.*, 1998, **39**, 2172.
- 59 P. Laverman, O. C. Boerman and G. Storm, *Methods Enzymol.*, 2003, **373**, 234–248.
- 60 A. L. B. de Barros, L. das Graças Mota, D. C. F. Soares, M. M. A. Coelho, M. C. Oliveira and V. N. Cardoso, *Bioorg. Med. Chem. Lett.*, 2011, **21**, 7373–7375.